RESEARCH PAPER

Block copolymers for the synthesis of pure and Bi-promoted nano-TiO$_2$ as active photocatalysts

D. Meroni · V. Pifferi · B. Sironi · G. Cappelletti · L. Falciola · G. Cerrato · S. Ardizzone

Abstract Nano-TiO$_2$ is certainly the most studied semiconductor for environmental purposes. Here, a template synthesis using block copolymers is combined to Bi promotion to the purpose of enhancing the TiO$_2$ photocatalytic activity by modulating the oxide surface area and porosity as well as by slowing down the electron–hole recombination. Three block copolymers of the Pluronic family, characterized by different micelle sizes in water as determined by light scattering analysis, are employed to induce mesoporosity in nano-TiO$_2$. The surfactants are removed by combining UV and thermal treatments to avoid pore collapse while obtaining a good oxide crystallinity. A fine modulation of pore size and total volume is obtained by changing polymer type and concentration, effectively enhancing the ability of the oxide to promote the mineralization of methylene blue stains. The mesoporous oxides are then used as scaffolds to obtain Bi$_2$O$_3$–TiO$_2$ composites.

X-ray diffraction, N$_2$ adsorption at subcritical temperatures, high-resolution transmission microscopy, Fourier transform infrared spectroscopy, and zeta potential determinations give insight on the composite structure and on the specificity of the Bi–mesoporous TiO$_2$ composites with respect to traditional sol–gel TiO$_2$ nanomaterials. All samples are tested for the photodegradation of methylene blue stains and of formic acid under dry and wet conditions, respectively. The presence of Bi promotes the photocatalytic activity of the final samples in both tested reactions (about 30 % mineralization enhancement with respect to unpromoted TiO$_2$). The top performing photocatalyst is the Bi$_2$O$_3$–mesoporous TiO$_2$, which shows the largest recombination time of photogenerated electrons and holes as determined by photocurrent measurements.

Keywords Pluronic block copolymers · Mesoporous nano-TiO$_2$ · Bi-promoted titania · Photocatalysis

D. Meroni · V. Pifferi · B. Sironi · G. Cappelletti · L. Falciola · S. Ardizzone (✉)
Dipartimento di Chimica Fisica ed Elettrochimica, Università di Milano, Via Golgi 19, 20133 Milan, Italy
e-mail: silvia.ardizzone@unimi.it

G. Cerrato
Dipartimento di Chimica IFM & NIS-Interdept. Excellence Centre, Università di Torino, Via Pietro Giuria, 7, 10125 Turin, Italy

Introduction

In the past decade, there has been a great interest in nanocrystalline titania materials. The photoelectronic properties of nano-titania are very promising for environmental or clean energy applications, such as photovoltaics and photocatalysis (Ardizzone et al. 2008; Crepaldi et al. 2003; Meroni et al. 2011).

Crystalline structure and particle morphology are responsible for an efficient light semiconductor interaction (Angelome et al. 2007).

Mesoporous TiO$_2$ materials with tailored pore size, high specific surface area, and well-defined crystalline frameworks have, therefore, great potential applications in these fields. The pore size and specific surface area greatly impact the physical properties of a mesoporous material and can play a relevant role in its activity (Bleta et al. 2010). For instance, Saadoun et al. (2000) reported that mesoporous anatase powder with larger pore diameter shows a higher photocatalytic activity, than the same system with smaller pores, for the degradation of formaldehyde under UV illumination. Even though formaldehyde is a small molecule, large pore diameters could provide a faster reaction pathway.

The synthesis of ordered mesoporous oxides goes back to the beginning of the 1990s when low molecular weight cationic surfactants were employed as structure-directing agents for the synthesis of mesoporous silica. In time this approach was extended to numerous systems using both anionic and non-ionic surfactants (Bates and Fredrickson 1999). A critical point of this kind of syntheses, especially in the case of titanium dioxide, is the control of the nucleation and growth processes and consequent crystallization taking place within the inorganic walls upon thermal treatment. When crystal size exceeds wall thickness, the continuous mesoporous structure usually collapses, leading to a fragile packing of nanocrystallites. A growing number of works was dedicated to the optimization of conditions leading to the production of ordered mesoporous nano-titania with efficient photocatalytic or photovoltaic performances. To this aim recently block copolymers have been consistently proposed (Wu and Rankin 2011). Block copolymers are made of two or more chemically distinct polymer blocks covalently bonded together (Alexandridis and Hutton 1995; Taylor et al. 2007). These blocks may be thermodynamically incompatible with each other supporting micro-phase separation on the molecular scale (in the nanometers range) to produce complex nanostructures with various morphologies depending on the relative volume fraction of one block with respect to the other (Tadros 2009).

The large majority of preparations of ordered mesoporous TiO$_2$ by block copolymers follows the evaporation-induced self-assembly (EISA) process, in which the polymers are introduced in the reaction mixture simultaneously with the titanium precursor (Brinker et al. 1999; Choi et al. 2004). Thus, condensation of the metal ions and self-assembly of the block copolymer templates occur simultaneously.

A novel method, termed the "nanoparticle route" (Bleta et al. 2010; Bosc et al. 2003), appears to be promising for the synthesis of stable mesostructured titania. In comparison with the classical EISA process, in the nanoparticle route, the copolymer is added to the titania nanoparticulate sol, and only the self-assembly process between copolymer and nanoparticles is allowed to take place. By this approach collapse problems that can be associated with template removal and crystallization may be reduced (Sanchez et al. 2008). Although the nanoparticles route method may imply a larger number of synthetic intermediate steps, it is inherently more flexible as every separate step can be tailored to produce the desired effect (promote surface area, given pore size, etc.). Further, presynthesized nanoparticles are used allowing a fine control of the material features (e.g., lattice location of dopants) (Wang et al. 2010).

In this study, a modified nanoparticle route is adopted. The TiO$_2$ uncalcined nanoparticles, separately prepared, are mixed with the selected copolymer in water. No mesophase of copolymer is allowed to form; since no long-range order of mesostructure is sought. The desired mesoporosity will, actually, be the result of the pores (voids) created into the oxide matrix by the micellar structures, decomposed during the calcination treatment. Three different block copolymers of the Pluronic family are employed and their self-aggregation behavior in water is studied. The role played by the different block molecular structure on the final morphological features of the oxide is investigated. The effect of mesoporosity on the resulting photocatalytic performances of the mesoporous oxides is examined, both directly onto the "dry" oxide and in solution. Furthermore, as the control over the morphological features of the host oxide may give rise to composite (i.e., mixed) oxides with improved features, mesoporous TiO$_2$ samples, obtained by the present procedure, are employed to obtain Bi-promoted TiO$_2$ samples. These latter materials are recently raising great interest in several fields like photocatalysis, photovoltaics, and hydrogen production (Jing et al. 2009; Shamaila et al. 2010). Indeed, Bi$_2$O$_3$ is a non-toxic and environmentally

friendly material which, thanks to its band structure (Bian et al. 2008), could trap photogenerated electrons, and thus improve the overall quantum efficiency of the material. In fact, theoretical calculations have shown that the specific band structure of Bi_2O_3–TiO_2 (Long and English 2009) significantly improves the oxide photocatalytic efficiency. Bi_2O_3 can thus represent a cheaper alternative to noble metals in enhancing the photocatalytic performances of TiO_2. Such theoretical results are supported, in the literature, by photoluminescence experiments (Shamaila et al. 2010) which showed a slowed radiative recombination process of photogenerated electrons and holes in Bi_2O_3–TiO_2 composites. However, no direct evidence of the actual reduced recombination rate can be found in the literature. Here, photocurrent measurements of Bi_2O_3–TiO_2 composites are performed to assess any effect of the Bi addition on the fate of the photogenerated electron–hole pair.

The use of mesoporous titania as a scaffold for Bi_2O_3 formation is an issue scantly investigated in the literature (Shamaila et al. 2010). Mesoporosity could enhance the dispersion of heteroatoms/oxide particles, determining a further improvement of the photocatalytic performances. In this study, the mesoporosity of the oxide is used to obtain highly dispersed Bi_2O_3–TiO_2 composites with enhanced photocatalytic activity. Their structural features and activity are compared with Bi_2O_3–TiO_2 composites, in which the titanium oxide is obtained by a traditional sol–gel reaction.

Experimental section

All the chemicals were of reagent grade purity and were used without further purification; double-distilled water passed through a Milli-Q apparatus was used to prepare solutions and suspensions. The Pluronics were obtained by courtesy of BASF Company (USA).

Synthesis of mesoporous titania

Titanium dioxide nanoparticles were synthesized by mixing the TiO_2 nanoparticle sol with a Pluronic copolymer in water.

The sol synthesis was performed as follows. A solution of 0.1 mol of $Ti(OC_3H_7)_4$ in 38 mL of 2-propanol was stirred for 10 min at 300 rpm at 25 °C. Then, 180 mL of water was added, dropwise, fast, to the alkoxide solution, to obtain a water/alkoxide molar ratio of 100 and a water/2-propanol molar ratio of 20. The slurry was stirred for 90 min to complete the hydrolysis. Subsequently, hydrochloric acid (HCl 37 %) was added to peptize the hydroxide precipitate to obtain a homogeneous milky suspension. The mixture was maintained under reflux at 80 °C for 5 h. The final product was a stable translucent suspension of TiO_2 nanoparticles. Preliminary studies showed that a separate HCl addition followed by a hydrothermal treatment allow to maximize the final sample surface area and porosity (Tables 1, 2, 3, 4).

A suitable amount of the chosen Pluronic (PEO_PPO_PEO, PEO = polyethylene oxide and PPO = polypropylene oxide) triblock copolymer (P104, F127, or P123) was then added to the sol after being liquefied in 2-propanol, and the mixture was maintained under stirring for 3 h at 50 °C. The ratio between the number of ethoxy units and the number of titanium moles (EO/Ti) was varied from 0 to 1.6. Xerogels were obtained after drying the sol by evaporation in a vacuum oven at 40 °C and 40 mbar, and they were calcined at 350 °C in static air for 5 h using a heating ramp of 3 °C min^{-1}. Finally, the powders were irradiated with UV light (iron halogenide lamp Jelosil HG 500, irradiation intensity reaching the sample: 30 mW cm^{-2}) for 5 h to remove the remaining traces of organic compounds. Samples are identified according to this notation: T_copolymer_(EO/Ti). For example, T_P104_1.2 indicates the use of the P104 copolymer, and an EO/Ti ratio

Table 1 Structural (anatase and brookite content, anatase crystallite sizes d_{101}^a) and morphological (BET surface area S_{BET}, total pore volume V_{pores}) features of bare titania samples

Sample	% Anatase	% Brookite	d_{101}^a (nm)	S_{BET} (m^2 g^{-1})	V_{pores} (mL g^{-1})
T	73	27	8	92	0.119
T_P104_0.5	62	38	8	147	0.352
T_P104_0.8	61	39	7	175	0.395
T_P104_1.0	74	26	7	178	0.398
T_P104_1.2	61	39	6	187	0.425
T_P104_1.4	61	39	6	205	0.429
T_P104_1.6	70	30	6	197	0.515
T_P123_1.2	59	41	6	199	0.391
T_F127_1.2	59	41	6	172	0.262

Table 2 Properties of Pluronic P104, P123, and F127 copolymers: average molecular weight, average composition, hydrophilic–lipophilic balance (HLB) (Taylor et al. 2007), and critical micelle concentration (as determined by surface tension measurements, see Online resources Fig. 2)

Pluronic copolymer	MM (g mol^{-1})	EO$_x$PO$_y$EO$_x$	HLB	CMC $\times 10^6$ (mol L^{-1})
P104	5,900	$x = 25$, $y = 56$	8	4.0
P123	5,750	$x = 20$, $y = 70$	7–12	3.1
F127	12,600	$x = 106$, $y = 70$	18–23	18.0

Table 4 Photocatalytic performances of bare and Bi-promoted TiO$_2$ samples for MB and formic acid mineralization

Sample	% MB mineralization	HCOOH dχ/dt (mS min^{-1})	τ (s)
Tsg	46 ± 1	0.51 ± 0.02	15
Tsg_Bi	68 ± 1	0.58 ± 0.01	16
T_P104_1.2	54 ± 1	0.48 ± 0.02	15
T_P104_1.2_Bi	78 ± 1	0.76 ± 0.01	19

Transient time constant (τ) extrapolated from the photocurrent measurements

of 1.2. Sol–gel TiO$_2$ samples were prepared by a classical sol–gel route (Boiadjieva et al. 2004; Carp et al. 2004) for the sake of comparison.

Synthesis of Bi–TiO$_2$ composites

Bi–TiO$_2$ materials were prepared by a direct impregnation method (Di Paola et al. 2002; Shamaila et al. 2010). Two calcined bare TiO$_2$ samples (a classical sol–gel sample, Tsg, and T_P104_1.2) were treated with a suitable amount of 0.1 M Bi(NO$_3$)$_3$ acidic solution. The starting molar ratio Bi/Ti was 0.02, on the grounds of previous literature results (Shamaila et al. 2010). Then, the powders were dried in oven and subsequently calcined at 350 °C in static air for 5 h using a heating ramp of 3 °C min^{-1}.

Samples characterization

Room-temperature X-ray powder diffraction (XRPD) patterns were collected between 10° and 80° with a Siemens D500 diffractometer, using Cu Kα radiation. Rietveld refinement has been performed using the GSAS software suite and its graphical interface EXPGUI. The average diameter of the crystallites, d,

was estimated from the most intense reflection (101) of the TiO$_2$ anatase phase using the Scherrer equation.

Specific surface areas were determined by the classical BET procedure using a Coulter SA 3100 apparatus. Desorption isotherms were used to determine the pore size distribution using the Barret–Joyner–Halander (BJH) method.

Diffuse reflectance spectra (DRS) of the powders were measured on a UV–Vis scanning spectrophotometer (Perkin-Elmer, Lambda 35) equipped with a diffuse reflectance accessory. A "total white" Perkin–Elmer reference material was used as reference.

Critical micelle concentrations in water of the employed block copolymers were determined at room temperature (RT) by surface tension measurement using the DuNouy method (TSD, Gibertini).

Micelle size distribution of different block copolymers was evaluated by Malvern Nano Zetasizer (ZEN 1600).

The temperature at which the complete decomposition of organics occurs in the TiO$_2$ xerogel was determined by TGA analysis (Perkin Elmer TGA 7).

Particles morphology was obtained by high-resolution transmission electron microscopy (HR-TEM), using a JEOL JEM 3010UHR (300 kV) microscope fitted with a LaB$_6$ single crystal filament and an Oxford INCA Energy TEM 200 energy dispersive

Table 3 Morphological features (BET surface area S_{BET}, total pore volume V_{pores}, content of pores with sizes ranging from 6 to 20 nm) of bare TiO$_2$ and Bi–TiO$_2$ composites

Sample	% Anatase	% Brookite	d_{101}^a (nm)	S_{BET} (mL g^{-1})	V_{pores} (mL g^{-1})	ζ potential (mV)
Tsg	70	30	7	150	0.338	−38
T_Bi	57	43	7	161	0.420	−10
T_P104_1.2	61	39	6	187	0.425	−35
T_P104_1.2_Bi	53	47	7	148	0.375	−23

X-ray (EDX) detector. All samples were dry deposited on Cu "holey" carbon grids (200 mesh).

Scanning electron microscopy (SEM, HITACHI TM-1000) equipped with EDX spectroscopy (Hitachi ED3000) was employed to estimate the Bi content in the composite samples.

Electrophoretic mobility and zeta potential data were obtained by a Coulter DELSA apparatus. The ionic strength of the suspensions was kept constant by $KNO_3 \times 10^{-2}$ M. Measurements were performed at pH 8 by a diluted KOH solution.

FTIR spectra (128 scans, 4 cm^{-1} resolution) were collected on a Bruker IFS 113v spectrometer, equipped with MCT detector. Samples were pressed into self-supporting pellets (approx 10–15 mg cm^{-2}) and placed in a quartz cell fitted with KBr windows. Prior to any FTIR measurements, all samples were activated in vacuo at either RT or at 250 °C, connecting the quartz cell to a conventional high vacuum glass line capable of a residual pressure <10^{-4} Torr (1 Torr = 133.32 Pa).

The photocatalytic activity of the samples was tested toward the mineralization of methylene blue on "dry" TiO_2 films and of formic acid in liquid medium, according to procedures previously described (Paoli et al. 2010; Spadavecchia et al. 2010). Films for formic acid degradation were prepared by depositing 0.1 g TiO_2 onto a rough Al substrate according to Ardizzone et al. 2011. Photocatalytic tests were carried out in an 850-mL thermostatic reactor containing 5×10^{-3} M formic acid solution. All degradation tests were carried out at 20 °C and at spontaneous pH in the experimental set-up under UV-A irradiation (3 h irradiation time). Methylene blue degradation tests were performed using TiO_2 films (0.08 g) deposited over glass slides (Milanesi et al. 2010) and stained with 0.25 mL of a methylene blue solution (0.02 M). The films were irradiated for 7 h under UV–A irradiation. The photon sources for both photocatalytic tests were provided by two 500 W iron halogenide lamps (Jelosil, model HG 500, 85 mW effective total power) emitting in the 315–400 nm wavelength range (UV–A). The actual mineralization of both formic acid and methylene blue were monitored by chemical oxygen demand (COD) measurements (Spectroquant Merck).

Photocurrent transient measurements (Hagfeldt et al. 1995) were performed in a suitable electrochemical cell with two platinum counter-electrodes placed in line with the working electrode in the middle. The saturated calomel reference electrode was placed orthogonally with a Luggin capillary, to minimize the ohmic drop. The electrodes were immersed in 0.5 M aqueous NaCl at a spontaneous pH and the cell was deaerated with nitrogen. The TiO_2 photoanodes were alternatively exposed to UV light (Jelosil HG 500). The photocurrent and the photocurrent transient were measured by a microIII Autolab potentiostat/galvanostat (EcoChemie, The Netherlands), at a constant potential. After a 60 s equilibration time in the dark under nitrogen degassing, dark/light alternations (200/100 s) were repeated for at least six times, to obtain reproducible transient patterns. The working electrodes were prepared depositing a film of eight thin layers (3 cm^2 surface area) of titania nanoparticles on an indium tin oxide (ITO) glass slide (by Aldrich), using a spin coating technique. The as-prepared films were finally sintered at 350 °C in air for 1 h.

Results and discussion

Synthesis of mesoporous TiO_2 samples

The presently adopted synthetic method is based on the occurrence of the self-assembly process between the copolymer and the nanoparticle precursors, separately prepared. The advantage of using preformed TiO_2 nanoparticles is that pre-condensed species exhibit a lower hydrolytic reactivity than molecular precursors, so that the chemistry, self-assembly, and processing parameters are more separated (Sanchez et al. 2008).

Three different copolymers of the Pluronic family (PEO_PPO_PEO, PEO = poly(ethylene oxide) and PPO = poly(propylene oxide)), characterized by diverse compositions and average molar mass, are adopted in template syntheses. The first part of this work, i.e., the optimization of the synthetic route and the study of the role played by EO/Ti ratio, was performed using P104 as the copolymer due to its relatively low molecular weight (around 6,000) and an intermediate HLB value (HLB = 8). This copolymer has not been previously adopted for the synthesis of TiO_2.

A tailored strategy for the removal of the template, after the synthesis, involving a mild heat treatment followed by UV irradiation, was developed to

maximize the sample porosity and surface area while allowing a complete removal of the template agent. The TG analysis under N_2 atmosphere of P104 shows that the copolymer is completely decomposed at about 300 °C (Fig. 1a). The TG analysis of uncalcined T_P104_1.2 shows a mass loss recorded below 150 °C, which can be attributed to the loss of physically adsorbed water, followed by two more separated mass losses (centered at about 220 and 270 °C) in the region where the polymer decomposition takes place. Although most of the copolymer is removed between 200 and 300 °C, a second much smaller weight loss takes place at around 400 °C (Fig. 1b). The degradation process ends at 420 °C, in agreement with what observed by Bleta et al. (2010) in
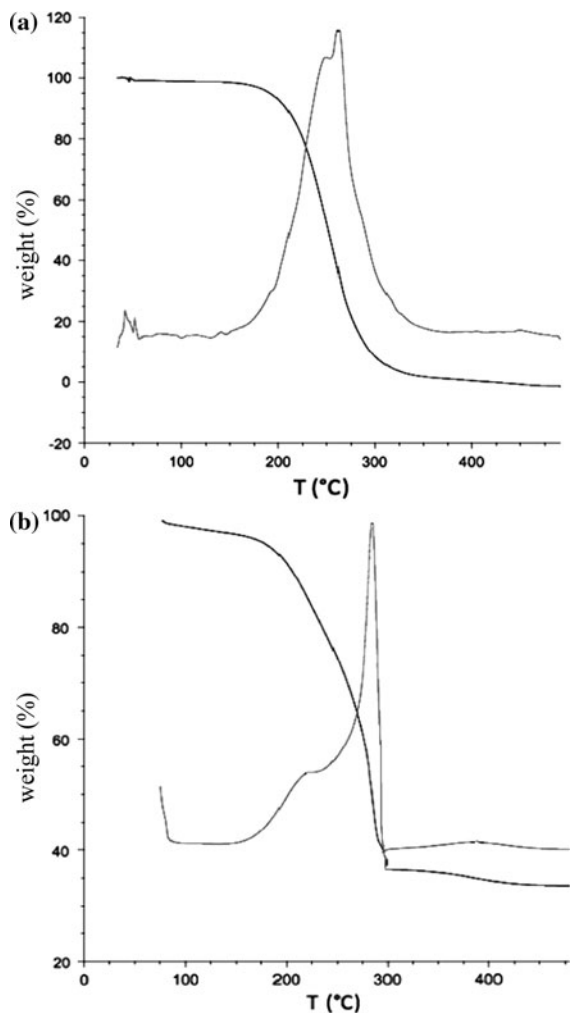
the case of TiO_2 templated by a different Pluronic polymer (F127). A calcination temperature of 350 °C with slow heating rate, under static air, was presently adopted to prevent a pore collapse due to the template removal. These calcination conditions are often employed in the literature (Bleta et al. 2010; Shamaila et al. 2010) to remove surfactants in oxide precursors; however, the TG analyses clearly show that not all the copolymer is decomposed at 350 °C. Thus, a subsequent UV irradiation treatment was presently performed to promote a complete template removal avoiding higher temperature-induced crystallite growth and a consequent pore collapse. The optimal time of UV irradiation was determined by surface area determinations: after 5 h UV irradiation, the sample surface area and pore volume reach a maximum value that is only negligibly improved by further irradiation. Moreover, HRTEM images (see the following) show that the sample pore walls are highly crystalline and that the crystallites are not aggregated.

The addition of the block copolymer results in a marked change in the morphological features of the oxide (Fig. 2). The reference sample (T), peptized in HCl without the addition of the copolymer and calcined under the same conditions, shows a N_2 adsorption–desorption isotherm with a type H2 hysteresis loop, which is typical of bottle-neck pores (Barrett et al. 1951; de Boer et al. 1966; Rouquerol et al. 1999). On the contrary, T_P104 samples present type IV isotherms (Fig. 2), characteristic of mesoporous materials (Bleta et al. 2010), with a type H1 hysteresis loop, typical of spherical or pseudospherical agglomerates with homogenous size and cylindrical

Fig. 1 TG analyses under N_2 atmosphere of **a** P104 copolymer and of **b** uncalcined T_P104_1.2
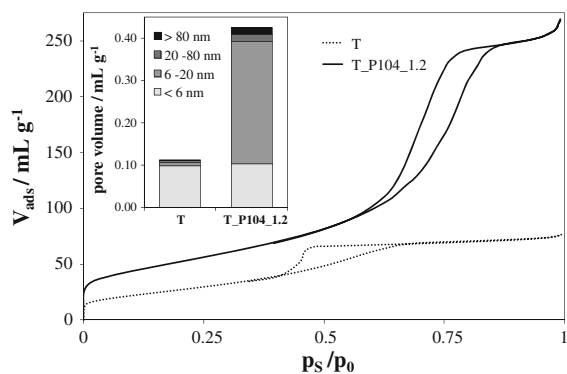
Fig. 2 N_2 adsorption–desorption isotherms at subcritical temperatures of T and T_P104_1.2 samples calcined at 350 °C. *Inset* relative pore volume distribution of the two samples

pores opened at both sides (Barrett et al. 1951; de Boer et al. 1966; Rouquerol et al. 1999). The addition of the copolymer also results in a remarkable increase in specific surface area and pore volume (Table 1). Such a large increase is mainly related to a narrowly distributed mesoporosity (Fig. 2, inset) that is almost absent in the reference sample.

Effect of the EO/Ti ratio

Different P104 copolymer concentrations, expressed as the ratio between the number of ethoxy units and the number of titanium atoms (EO/Ti), were tested. All obtained samples are anatase–brookite composites. No rutile phase was found as expected from the adopted low calcination temperatures. The formation of the brookite polymorph usually occurs together with anatase for crystallites of small size (Boiadjieva et al. 2004). The surfactant addition seems to cause a slight enrichment in the brookite phase (Table 1, Columns 2–3) and a slight decrease in the average crystallite diameter (Table 1, Column 4). Varying the copolymer amount modifies significantly the sample morphological features: at increasing EO/Ti ratios, a steady increase of the sample surface area and pore volume is observed (Table 1, Columns 5–6). However, the average pore dimension remains almost unchanged (7 nm) for all tested EO/Ti ratio, and a narrow size distribution (65–70 % pores with a size in the 6–10-nm range) is obtained for all samples.

At the highest tested concentrations, the copolymer removal becomes more demanding and progressively longer UV irradiation times are requested to obtain its complete removal. Therefore, an optimal concentration (EO/Ti 1.2), allowing a fast and complete removal together with high surface area and mesoporosity, was adopted for testing the other two copolymers.

Effect of the copolymer type

Three different Pluronic copolymers were tested to investigate the role played by the different block structure on the oxide final features. The adopted copolymers were two widely employed structure-directing agents (P123, F127) (Bleta et al. 2010; Bosc et al. 2003; Crepaldi et al. 2003; Sanchez et al. 2008), together with the already described P104. The characteristics of the three copolymers are reported in Table 2. The samples obtained using the same EO/Ti ratio but different templating agents show different shapes of N_2 adsorption–desorption hysteresis loops (Online Resources Fig. 1).

During the syntheses, the adopted copolymer concentrations were at least two orders of magnitude higher than the measured critical micelle concentration (Table 2, Online Resources, Fig. 2). The copolymers were characterized for their CMC by surface tension measurements (Table 2). The values reported in the literature fall in broad ranges and are strongly affected by the method adopted for the CMC determination (Perry et al. 2011; Tsui et al. 2008, 2010). In the case of P123 the present value closely compares with the values reported by Kadam et al. (2011) and by Lee et al. (2011). In the case of F127, both larger and lower CMC values, with respect to the present one, can be found in the literature (Alexandridis et al. 1994; Hecht and Hoffmann 1995; Zana et al. 2006) while for P104 the literature data are very limited and significant comparisons cannot be made.

The rapid solvent evaporation adopted in this study does not allow a mesostructure to be formed. Therefore, the pore morphology is determined only by the micelle features. Figure 3a shows the micelle size distribution for the three polymers as determined by light scattering at the polymer concentrations adopted in the syntheses. Both P104 and P123 present a monomodal size distribution centered around 10–15 nm, in agreement with literature data (Alexandridis et al. 1995; Lee et al. 2011). Instead, in the case of F127, more than one component can be appreciated besides the main population at small sizes. Actually, the sequence shown by the pore sizes in the mesoporous oxides (Fig. 3b) reflects the sequence among the principal populations of micelle sizes. In the case of F127, only one pore size component is appreciable possibly because the larger micelle sizes lead to pores out of the mesoporosity range. The obtained oxides show a narrowly distributed mesoporosity that reflects the sequence of the micelle dimensions, as determined by light scattering (Fig. 3a).

All obtained samples were tested toward the photocatalytic oxidation of methylene blue. All the mesoporous samples, with the exception of T_P104_0.5, give mineralization degrees higher than those of reference sample T (mineralization percentage 45) and of the traditional photocatalytic commercial sample Degussa P25 (38 %). Figure 4 reports the mineralization percentage as a function of the sample surface area. The mineralization degree shows a good linear correlation
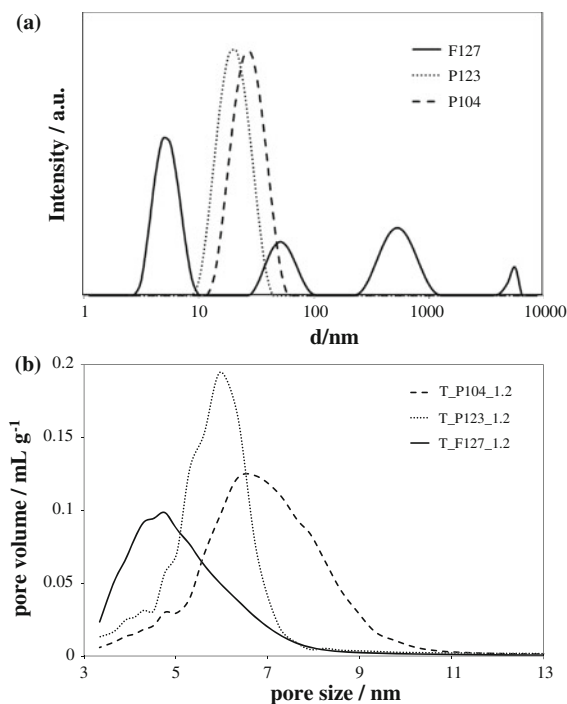
Fig. 3 **a** Micelle size distribution by light scattering for the three types of Pluronic and **b** pore size distribution of the calcined TiO_2 powders by nanoparticle route in the presence of the adopted copolymers
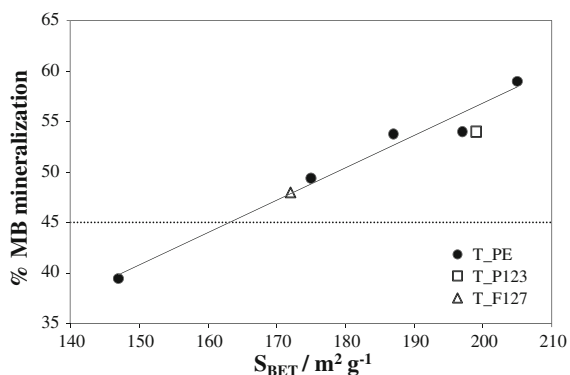
Fig. 4 % MB mineralization as a function of the surface area of the TiO_2 samples

with the sample surface areas that is irrespective of the type of copolymer employed. Thus, the mineralization degree seems, in this case, to be directly affected by the specific surface area and only indirectly by the sample pore size distribution. It is not surprising that the surface area of the photocatalyst plays a pivotal role in the case of self-cleaning of dry surfaces, like in the tested

degradation of methylene blue stains. A higher photocatalyst surface area leads to a larger extent of pollutant directly adsorbed at the oxide surface and thus to a faster oxidation as the degradations probably occurs via a direct oxidation at the catalyst surface. Therefore, in this case, the diffusion of the pollutant into the photocatalyst pore network is less crucial.

Bi–TiO$_2$ composites

Due to the environmentally friendly nature of Bi (and of its compounds) and to the favorable semiconductor features of Bi_2O_3, Bi-promoted TiO_2 samples were obtained with the aim to improve their photocatalytic performance. Bi_2O_3–TiO_2 composites were synthesized by using as scaffolds both the mesoporous TiO_2 and also a TiO_2 powder obtained by a classical sol–gel route to highlight possible effects introduced by the mesoporous structure of the host oxide. Comparing the effect of the different adopted copolymers, it emerges (Table 1) that the samples treated with P104 have the largest total pore volume: all the T_P104 samples, with the exception of T_P104_0.5, show a higher pore volume than T_P123 and T_F127 samples. Moreover, P104 leads to larger pores with respect to the other tested copolymers in agreement with the observed unimodal micelle sizes. The P104 copolymer was thus chosen to prepare Bi-doped mesoporous TiO_2 composites.

For all Bi-promoted oxides, peaks relative to separate Bi_2O_3 phases are not appreciable in X-ray diffraction patterns, while Bi species can be observed by EDX in Bi/Ti atomic ratios (corresponding to a weight percentage of about 10) comparable with those adopted in the synthesis. The presence of Bi slightly promotes the TiO_2 brookite polymorph while no variations on the crystallite sizes are observed (Table 3). Although the surface area of the mesoporous sample is larger (about 20 %) than the sol–gel one, the effects produced by the Bi addition are opposite for the two oxide synthetic routes. In the case of the sol–gel sample, the presence of Bi produces a slight increase in the specific surface area and an appreciable increase in the total pore volume possibly due to a better dispersion of the TiO_2 particles in the strong acid medium used for the impregnation. Instead, in the case of the mesoporous TiO_2 both the surface area and the total pore volume decrease appreciably. This effect could be traced back to the desired partial filling of the mesopores by Bi_2O_3. Figure 5 reports the comparison
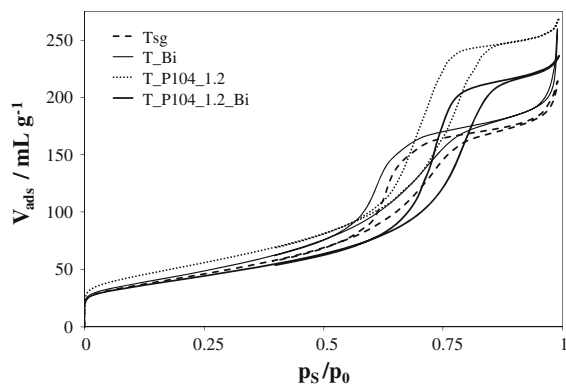
Fig. 5 N$_2$ adsorption–desorption isotherms of bare (Tsg and T_P104_1.2) and Bi-promoted (Tsg_Bi and T_P104_1.2_Bi) titania samples

among the N$_2$ adsorption/desorption isotherms of two bare TiO$_2$ samples (sol–gel and mesoporous) and of the two relative samples promoted by Bi. In the case of the sol–gel samples, the isotherms show the presence of capillary condensation in the mesopores but eventually give rise to the sharp increase of adsorbed volume at relative pressures close to 1, indicating the presence in the samples of both mesoporosity and of a non-porous surface (Barrett et al. 1951; de Boer et al. 1966; Rouquerol et al. 1999). The pore shape changes drastically from type H1 in mesoporous samples, typical of cylindrical pores, to H2 in sol–gel samples, representative of bottle-neck pores (Barrett et al. 1951; de Boer et al. 1966; Rouquerol et al. 1999). The presence of Bi does not modify the shape of the isotherms loop but the shift of the T_P104_1.2Bi curve to lower volumes with respect to T_P104_1.2, is a direct indication of a partial filling of the mesopores by the bismuth oxide.

The addition of Bi to the synthesis slightly modifies the shape of DRS curves (Online Resources, Fig. 3). The observed shift of the Bi-promoted curve suggests the formation of intra-gap localized levels (Shamaila et al. 2010).

HRTEM (Fig. 6) investigations indicate that all samples are characterized by a small size of the crystallites (5–8 nm), in good agreement with the data obtained by means of X-ray diffraction (see Table 1). Smooth edges and high transparency to the electron beam are appreciable as well as a good crystallinity, as indicated by the high incidence of fringe patterns, generated by the presence of crystalline planes exhibiting low *hkl* indexes. A detailed inspection of the
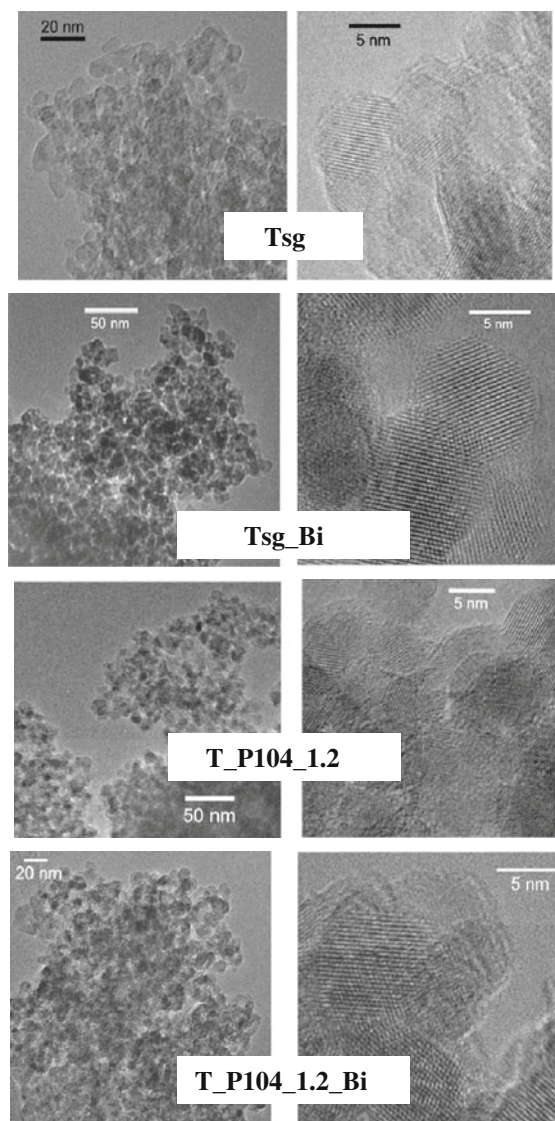
Fig. 6 HRTEM micrographs of pure and Bi-promoted titania powders

fringes evidences that for all samples the particles exhibit the same type of crystal planes. The lattice spacings indicate as main termination the (101) crystal plane of anatase (JCPDS file n. 21-1272), with a less frequent presence of the (111) crystal plane of brookite (JCPDS file n. 2-514) (Xu and Zhang 2009). In any case, but more frequently for the systems synthesized employing the P104 copolymer, the presence of Bi is linked to a general underestimation of the lattice distances ascribable to the (111) crystal plane of the brookite phase. Although no clear diffraction pattern

relative to bulk Bi_2O_3 can be appreciated in both HRTEM and XRD, the above-mentioned distortion of the lattice distances can be most likely attributed to the presence of a highly nano-dispersed oxide phase containing Bi species. This conclusion is also supported by other indirect determinations described in the following.

In order to characterize the surface terminations present onto the nanoparticles of these various TiO_2-based systems, FTIR spectroscopy of the powders themselves has been resorted to. All the results are reported in Fig. 7, in which the full lines refer to a plain vacuum activation at RT (namely, IR beam temperature, some 30 °C higher than RT), whereas the bold lines refer to a vacuum activation carried out at 250 °C (to get rid of all physisorbed and/or weakly adsorbed surface species). Some spectral features deserve comments, as reported in the following:

1. For all spectra relative to the plain RT evacuation, a broad envelope is present in the 2,500–3,500 cm^{-1} range. This is not surprising, as at the surface of all these TiO_2-based systems a huge amount of OH species interacting by H bonding are present and this envelope represents the v_{OH} mode of all these species (Little 1966). The spectroscopic δ_{HOH} counterpart of these species is represented by the band located at ~ 1620 cm^{-1} and indicated by an arrow in Fig. 7. All the above spectral components are absent (or drastically reduced) after the activation at 250 °C, as this thermal treatment carries out a dehydration (up to a medium degree) of the oxidic surface.

2. At higher frequency ($v > 3,600$ cm^{-1}) an envelope of singled out components is evident in all cases: these components are better observable in the bold curves, when the surface has reached a medium degree of dehydration. In fact, all these bands are ascribable to the v_{OH} modes of OH species free from H-bonding interaction (Morterra et al. 1989) and are better observable in the blown-up section reported in the inset to Fig. 7. In particular, it can be noted that, for the plain TiO_2 system (see the uppermost curve in the inset) obtained by sol–gel synthesis, at least three different components can be singled out. When Bi species are added, the three components are still observable, even though with a different intensity ratio. On the other hand, in the case of

the systems obtained employing the P104 copolymer, there is a general lowering of the quality of the spectra (see the lower couple of curves in the inset), much more marked when Bi species are present. In the latter case, only the highest component is still observable and its intensity represents only a small fraction of the original band. These observations allow us to draw some preliminary conclusions about the location of Bi species; in particular, their presence seems to be linked to the covering and/or disappearance of some specific band ascribable to OH species. This may indicate that the grafting of Bi species is most likely due to the "consumption" of surface OH species in the TiO_2 matrix.

3. In the cases of the pure TiO_2 oxides, no matter the synthetic route followed for the preparation, some peculiar absorption located in the 3,000–2,750 cm^{-1} range are evident. These are ascribable to the v_{CH} mode of hydrocarbonaceous species chemisorbed at the surface of the oxide as a results of the synthetic route and/or to the exposure to the atmosphere after the calcinations treatment (Magnacca et al. 2003).

The interfacial electrification features of the oxides were analyzed by zeta potential measurements in aqueous suspensions. At pH 8, the Bi composites show zeta potential values which are less negative than those of the undoped TiO_2 samples (Table 3). Such effect can be traced back to a shift of the isoelectric point (i.e.p.) in the alkaline direction, with respect to the i.e.p. of bare TiO_2 (pH ≈ 6) due to the presence of Bi_2O_3. Actually the isoelectric point of pure Bi_2O_3 is located at pH 9 (Kosmulski 2009). The effect is larger in the case of the sol–gel sample, possibly due to a larger surface extension of the Bi oxide as suggested by the larger surface area of T_Bi with respect to both Tsg and T_P104_1.2_Bi.

Bi_2O_3–TiO_2 composites photocatalytic activity

The photocatalytic activity of Bi_2O_3–TiO_2 composites was tested with respect to the mineralization of both MB deposited onto the dry oxide and of formic acid in the liquid phase (Table 4). The mineralization (total degradation) of MB to CO_2 for the sol–gel sample is lower than in the case of the mesoporous one. In both the cases, the promotion by Bi produces an increased mineralization.

Fig. 7 FTIR spectra of bare (Tsg and T_P104_1.2) and Bi-promoted (Tsg_Bi and T_P104_1.2_Bi) titania samples. *Full lines* activation in vacuo at RT, *bold lines* activation in vacuo at 250 °C)
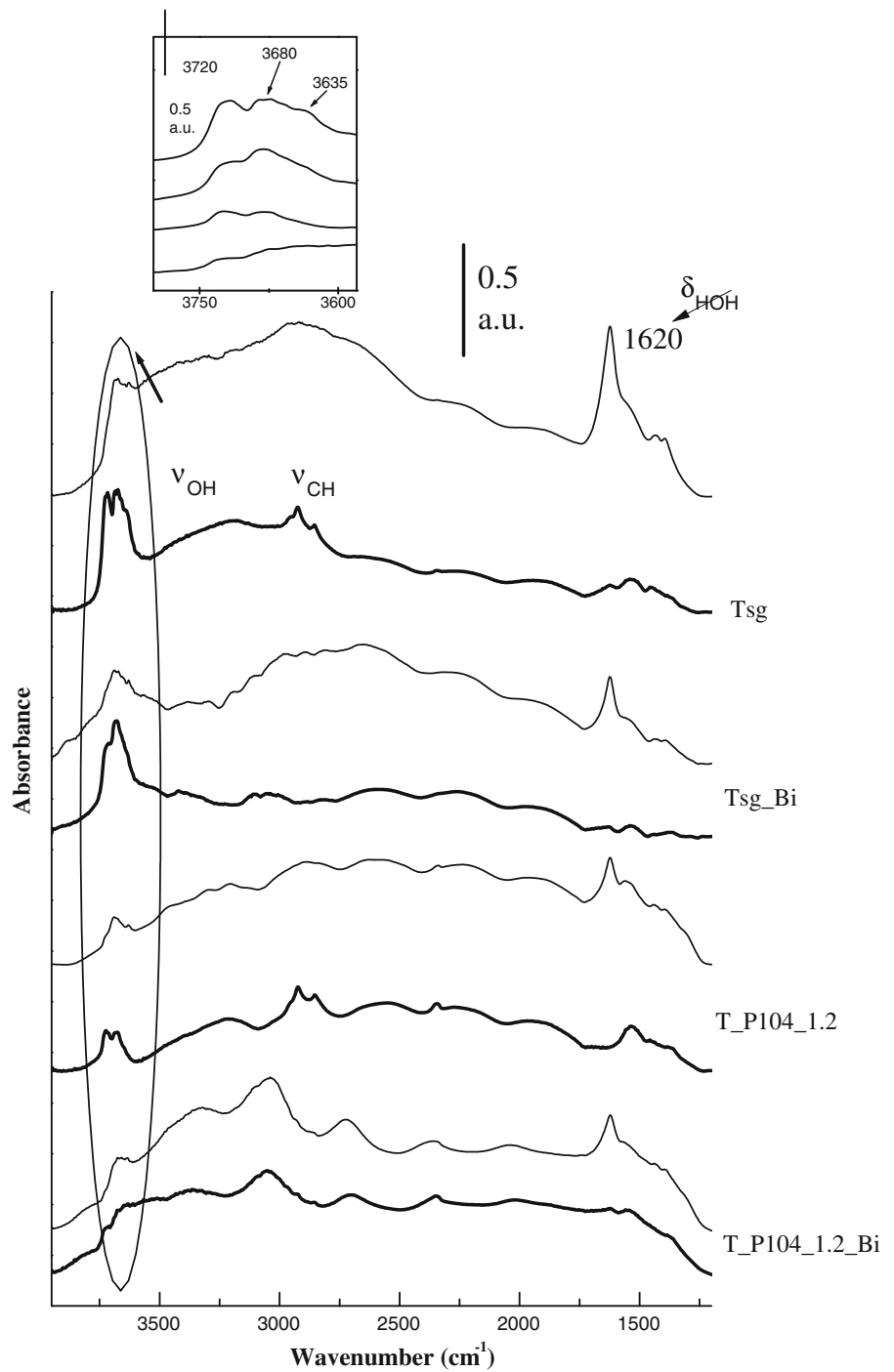
In liquid phase, all samples show a mineralization degree larger than 80 % at 3 h reaction time, while conductivity variations allow differences among the various samples to be appreciated (Table 4, third column). The slope of the χ versus t plot represents the rate of conductivity decrease due to the progressive

disappearance of formic acid. The slope increases for both Bi-promoted samples, the more so in the case of T_P104_1.2_Bi.

On the grounds of what reported above Bi_2O_3–TiO_2 composites show much higher photocatalytic activity than bare TiO_2 both as a dry oxide and in liquid phase tests. It may be relevant to recall that, while in the case of the sol–gel sample the addition of Bi induces an increase in the oxide surface area, thus producing a larger extension of photocatalyst in the reactions, the Bi-promoted mesoporous sample is the one showing at the same time the lowest surface area and the top photocatalytic performances.

Possibly, this effect is to be connected to a lower recombination between electrons and holes due to a better separation between the two oxide phase domains. Photocurrent measurements are performed to further analyze this latter point. The probability in charge recombination was studied by photocurrent kinetics curves (inset of Fig. 8). The photocurrent decay indicates that electron–hole recombination processes are occurring. The photocurrent transient can be evaluated by considering the kinetic equation

$$\ln(D) = -t/\tau,$$

where $D = \frac{I(t)-I(st)}{I(in)-I(st)}$; τ is the transient time constant, which indicates the time of recombination process; $I(t)$ is the current at time t; $I(st)$ is the stationary current, and $I(in)$ is the current at $t = 0$.

Figure 8 shows the comparison between $\ln(D)$ versus time plot of Tsg and Tsg_Bi. The linear behavior observed for all the tested materials indicates that the decay mechanism is due only to surface recombination leading to a first-order kinetics in electrons surface
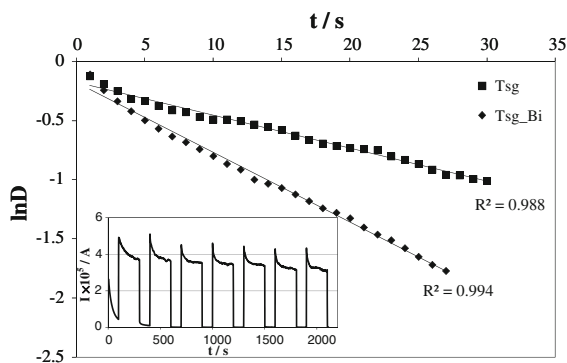
Fig. 8 $\ln(D)$ versus time plot of Tsg and Tsg_Bi. *Inset* photocurrent kinetic curve relative to Tsg_Bi

concentration (Dholam et al. 2010; Tafalla et al. 1990); the different slopes supports a longer recombination time for the Bi-promoted sample.

The transient time constant (τ) reported in Table 4 for the adopted samples are larger (15–20 s) than those observed by compact single-crystal or polycrystalline electrodes (few milliseconds, Dholam et al. 2010; O'Regan et al. 1990), but comparable with what reported by other authors in the case of both pure and doped nano-titania photocatalysts (Dholam et al. 2010). The τ values of the Bi-promoted samples (Table 3) are slightly better than those of the undoped ones, especially in the case of T_P104_1.2_Bi, in which the controlled mesopores are filled by bismuth oxide, leading to a better charge separation efficiency. Thus, the addition of bismuth in a tailored mesoporous titania structure enhances the photocatalytic efficiency, as demonstrated by the mineralization tests. The optimal amount of Bi presently selected is the result of a balance between the enhancement of the charge separation efficiency and the reduction of the sample surface area. Increasing Bi/Ti ratio above 2 % results in a marked decrease in surface area (25 % passing from 1 to 3 %) that reduces the photocatalytic activity of the sample in agreement with literature results (Shamaila et al. 2010).

Conclusions

Block copolymers of the Pluronic family (P104, P123, and F127) successfully induce mesoporosity in nano-TiO_2 samples. The procedure adopted for the surfactant removal, a combination of thermal treatments and UV irradiation steps, permits to avoid pore collapse as well as to obtain a good degree of crystallinity. The sequence of the mesopore sizes in the samples obtained by different Pluronic copolymers follows the sequence of the relative micelle size in water, measured in the same conditions of the oxide formation. Copolymers characterized by relatively low molecular weights (around 6,000) and by intermediate HLB values (P104 and P123) induce larger surface areas and pore volumes with respect to another Pluronic molecule (F127), characterized by a twice as large MW and a more relevant hydrophilic component. P104, used in the present case for the first time in the synthesis of nano-TiO_2, appears to be the best promoter of mesoporosity, producing increases in both

surface area and total pore volume starting from very low copolymer initial amounts.

Bi-promoted oxides were prepared using as scaffolds pre-calcined TiO_2 samples. For the sake of comparison both the mesoporous and a "classic" sol–gel TiO_2 sample were employed. XRPD lines do not confirm the presence of bulk Bi_2O_3 but HRTEM micrographs show effects possibly linked to a highly monodispersed bismuth oxide into the titania matrix. Furthermore, EDX analyses support the presence of Bi in the final samples in the same Bi/Ti ratio as the one adopted in the synthesis. Definite differences appear when comparing the sol–gel and mesoporous Bi-promoted samples. In the latter case, a decrease in surface area and pore volume suggests the desired formation of Bi_2O_3 in the voids created by the mesoporosity. Both FTIR and zeta potential measurements show that the Bi/Ti interactions are mainly localized at the surface of the titania particles.

The presence of Bi promotes the photocatalytic activity of the final samples. The top performing photocatalyst is the Bi_2O_3–mesoporous TiO_2, both for the degradation of methylene blue onto the dry oxide and for the degradation of formic acid in the liquid phase. Photocurrent measurements show that the recombination time between electrons and holes is the largest in the case of this sample. Apparently, the prevailing location of Bi_2O_3 in the mesopores allows the formation of separate Bi_2O_3/TiO_2 domains; this occurrence could promote an increase in charge separation efficiency due to interfacial electron transfer via the junction between TiO_2 and Bi_2O_3 nano-crystals. Bi_2O_3 may further, due to its band structure, act as an electron acceptor which aids the effective separation between electron and hole pairs.

References

Alexandridis P, Hutton TA (1995) Poly(ethylene oxide)–poly(propylene oxide)–poly(ethylene oxide) block-copolymer surfactants in aqueous-solutions and at interfaces—thermodynamics, structure, dynamics, and modeling. Colloids Surf A 96:1–46. doi:10.1016/0927-7757(94)03028-X

Alexandridis P, Holzwart JF, Hatton TA (1994) Micellization of poly(ethylene oxide)–poly(propylene oxide)–poly(ethylene oxide) triblock copolymers in aqueous-solutions—thermodynamics of copolymer association. Macromolecules 27:2414–2425. doi:10.1021/ma00087a009

Alexandridis P, Nivaggioli T, Hatton TA (1995) Temperature effects on structural-properties of pluronic P104 and F108 PEO–PPO–PEO block-copolymer solutions. Langmuir 11:2847–2848. doi:10.1021/la00007a085

Angelome P, Andrini L, Calvo ME, Requejo FG, Bilmes SA, Soler-Illia GJAA (2007) Mesoporous anatase TiO_2 films: use of TiK XANES for the quantification of the nanocrystalline character and substrate effects in the photocatalysis behavior. J Phys Chem C 111:10886–10893. doi:10.1021/jp069020z

Ardizzone S, Bianchi CL, Cappelletti G, Naldoni A, Pirola C (2008) Photocatalytic degradation of toluene in the gas phase: relationship between surface species and catalyst features. Environ Sci Technol 42:6671–6676. doi:10.1021/es8009327

Ardizzone S, Cappelletti G, Meroni D, Spadavecchia F (2011) Tailored TiO_2 layers for the photocatalytic ozonation of cumylphenol, a refractory pollutant exerting hormonal activity. Chem Commun 47:2640–2642. doi:10.1039/c0cc05134a

Barrett EP, Joyner LG, Halenda PH (1951) The determination of pore volume and area distributions in porous substances. I. Computations from nitrogen isotherms. J Am Chem Soc 73:373–380. doi:10.1021/ja01145a126

Bates FS, Fredrickson GH (1999) Block copolymers—designer soft materials. Phys Today 52:32–38. doi:10.1063/1.882522

Bian ZF, Zhu J, Wang SH, Cao Y, Qian XF, Li HX (2008) Self-assembly of active Bi_2O_3/TiO_2 visible photocatalyst with ordered mesoporous structure and highly crystallized anatase. J Phys Chem C 112:6285–6286. doi:10.1021/jp800324t

Bleta R, Alphonse P, Lorenzato L (2010) Nanoparticle route for the preparation in aqueous medium of mesoporous TiO_2 with controlled porosity and crystalline framework. J Phys Chem C 114:2039–2048. doi:10.1021/jp909646h

Boiadjieva T, Bianchi CL, Cappelletti G, Ardizzone S, Rondinini S, Vertova A (2004) The role of surface electrification on the growth and structural features of titania nanoparticles. Phys Chem Chem Phys 6:3535–3539. doi:10.1039/b402370f

Bosc F, Ayral A, Albouy PA, Guizard C (2003) A simple route for low-temperature synthesis of mesoporous and nanocrystalline anatase thin films. Chem Mater 15:2463–2468. doi:10.1021/cm031025a

Brinker CJ, Lu Y, Sellinger A, Fan H (1999) Evaporation-induced self-assembly: nanostructures made easy. Adv Mater 11:579–585. doi:10.1002/(SICI)1521-4095(199905)11:7<579:AID-ADMA579>3.0.CO;2-R

Carp O, Huisman CL, Reller A (2004) Photoinduced reactivity of titanium dioxide. Progr Solid State Chem 32:33–117. doi:10.1016/j.progsolidstchem.2004.08.001

Choi SY, Mamak M, Coombs N, Chopra N, Ozin GA (2004) Thermally stable two-dimensional hexagonal mesoporous nanocrystalline anatase, meso-nc-TiO_2: bulk and crack-free thin film morphologies. Adv Funct Mater 14:335–344. doi:10.1002/adfm.200305039

Crepaldi EL, Soler Illia GJDAA, Grosso D, Castagnol F, Ribot F, Sanchez C (2003) Controlled formation of highly

organized mesoporous titania thin films: from mesostructured hybrids to mesoporous nanoanatase TiO$_2$. J Am Soc 125:9770–9786. doi:10.1021/ja030070g

de Boer JH, Lippens BC, Linsen BG, Broekhof JCP, van den Heuvel A, Osinga TJ (1966) Thet-curve of multimolecular N$_2$-adsorption. J Colloid Interface Sci 21:405–414. doi:10.1016/0095-8522(66)90006-7

Dholam R, Patel N, Santini A, Miotello A (2010) Efficient indium tin oxide/Cr-doped-TiO$_2$ multilayer thin films for H$_2$ production by photocatalytic water-splitting. Int J Hydrogen Energy 35:9581–9590. doi:10.1016/j.ijhydene.2010.06.097

Di Paola A, Marcì G, Palmisano L, Schiavello M, Uosaki K, Ikeda S, Ohtani B (2002) Preparation of polycrystalline TiO$_2$ photocatalysts impregnated with various transition metal ions: characterization and photocatalytic activity for the degradation of 4-nitrophenol. J Phys Chem B 106:637–645. doi:10.1021/jp013074l

Hagfeldt A, Lindström H, Södergren S, Linquist S-E (1995) Photoelectrochemical studies of colloidal TiO$_2$ films—the effect of oxygen studied by photocurrent transients. J Elecroanal Chem 381:39–46. doi:10.1016/0022-0728(94)03622-A

Hecht E, Hoffmann H (1995) Kinetic and calorimetric investigations on micelle formation of block-copolymers of the poloxamer type. Colloids Surf A 96:181–197. doi:10.1016/0927-7757(94)03044-Z

Jing L, Wang J, Qu Y, Luan Y (2009) Effects of surface-modification with Bi$_2$O$_3$ on the thermal stability and photoinduced charge property of nanocrystalline anatase TiO$_2$ and its enhanced photocatalytic activity. Appl Surf Sci 256:657–663. doi:10.1016/j.apsusc.2009.08.037

Kadam Y, Yerramilli U, Bahadur A, Bahadur P (2011) Micelles from PEO–PPO–PEO block copolymers as nanocontainers for solubilization of a poorly water soluble drug hydrochlorothiazide. Colloids Surf B 83:49–57. doi:10.1016/j.colsurfb.2010.10.041

Kosmulski M (2009) Compilation of PZC and IEP of sparingly soluble metal oxides and hydroxides from literature. Adv Colloid Interface Sci 152:14–25. doi:10.1016/j.cis.2009.08.003

Lee ES, Oh YT, Youn YS, Nam M, Park B, Yun J, Kim JH, Song H-T, Oh KT (2011) Binary mixing of micelles using Pluronics for a nano-sized drug delivery system. Colloids Surf B 82:190–195. doi:10.1016/j.colsurfb.2010.08.033

Little LH (1966) Infrared spectra of adsorbed species. Academic Press, London

Long R, English NJ (2009) Synergistic effects of Bi/s codoping on visible light-activated anatase TiO$_2$ photocatalysts from first principles. J Phys Chem C 113:8373–8377. doi:10.1021/jp900589k

Magnacca G, Cerrato G, Morterra C, Signoretto M, Somma F, Pinna F (2003) Structural and surface characterization of pure and sulfated iron oxides. Chem Mater 15:675–687. doi:10.1021/cm021268n

Meroni D, Ardizzone S, Cappelletti G, Oliva C, Ceotto M, Poelman D, Poelman H (2011) Photocatalytic removal of ethanol and acetaldehyde by N-promoted TiO$_2$ films: the role of the different nitrogen sources. Catal Today 161:169–174. doi:10.1016/j.cattod.2010.08.013

Milanesi F, Cappelletti G, Annunziata R, Bianchi CL, Meroni D, Ardizzone S (2010) Siloxane-TiO$_2$ hybrid nanocomposites. The structure of the hydrophobic layer. J Phys Chem C 114:8287–8293. doi:10.1021/jp1014669

Morterra C, Bolis V, Fisicaro E (1989) The hydrated layer and the adsorption of co at the surface of TiO$_2$ (anatase). Colloids Surf 41:177–188. doi:10.1016/0166-6622(89)80051-4

O'Regan B, Moser J, Anderson M, Grätzel M (1990) Vectorial electron injection into transparent semiconductor membranes and electric-field effects on the dynamics of light-induced charge separation. J Phys Chem 94:8720–8726. doi:10.1021/j100387a017

Paoli E, Cappelletti G, Falciola L (2010) Electrochemistry as a tool for nano-TiO$_2$ deposition and for photoremediation pollutant monitoring. Electrochem Commun 12:1013–1016. doi:10.1016/j.elecom.2010.05.012

Perry CC, Sabir TS, Livingston WJ, Milligan JR, Chen Q, Maskiewicz V, Boskovic DS (2011) Fluorescence of commercial Pluronic F127 samples: temperature-dependent micellization. J Colloid Interface Sci 354:662–669. doi:10.1016/j.jcis.2010.10.028

Rouquerol J, Rouquerol F, Sing KSW (1999) Adsorption by powders and porous solids. Academic Press, London

Saadoun L, Ayllon JA, Jimenez-Becerril J, Peral J, Domenech X (2000) Synthesis and photocatalytic activity of mesoporous anatase prepared from tetrabutylammonium–titania composites. Mater Res Bull 35:193–202. doi:10.1016/S0025-5408(00)00204-X

Sanchez C, Boissière C, Grosso D, Laberty C, Nicole L (2008) Design, synthesis, and properties of inorganic and hybrid thin films having periodically organized nanoporosity. Chem Mater 20:682–737. doi:10.1021/cm702100t

Shamaila S, Sajjad AKL, Chen F, Zhang J (2010) Bismuth-doped ordered mesoporous TiO$_2$: visible-light catalyst for simultaneous degradation of phenol and chromium. Chem Eur J 16:13795–13804. doi:10.1002/chem.201001099

Spadavecchia F, Cappelletti G, Ardizzone S, Bianchi CL, Cappelli S, Oliva C, Scardi P, Leoni M, Fermo P (2010) Solar photoactivity of nano-N–TiO$_2$ from tertiary amine: role of defects and paramagnetic species. Appl Catal B 96:314–322. doi:10.1016/j.apcatb.2010.02.027

Tadros T (2009) Polymeric surfactants in disperse systems. Adv Colloid Interface Sci 147–148:281–299. doi:10.1016/j.cis.2008.10.005

Tafalla D, Salvador P, Benito RM (1990) Kinetic approach to the photocurrent transients in water photoelectrolysis at n-TiO$_2$ electrodes. Analysis of the photocurrent-time dependence. J Electrochem Soc 137:1810–1815. doi:10.1149/1.2086809

Taylor DJF, Thomas RK, Penfold J (2007) Polymer/surfactant interactions at the air/water interface. Adv Colloid Interface Sci 132:69–110. doi:10.1016/j.cis.2007.01.002

Tsui HW, Hsu YH, Wang JH, Chen LJ (2008) Novel behavior of heat of micellization of Pluronics F68 and F88 in aqueous solutions. Langmuir 24:13858–13862. doi:10.1021/la803272y

Tsui HW, Wang JH, Hsu YH, Chen LJ (2010) Study of heat of micellization and phase separation for Pluronic aqueous solutions by using a high sensitivity differential scanning

calorimetry. Colloid Polym Sci 288:1687–1696. doi:10.1007/s00396-010-2308-5

Wang JS, Li H, Li HY, Zou C (2010) Mesoporous TiO$_{(2-x)}$A$_{(y)}$ (A = N, S) as a visible-light-response photocatalyst. Solid State Sci 12:490–497. doi:10.1016/j.solidstatesciences.2009.12.01

Wu QL, Rankin SE (2011) Tuning the mesopore size of titania thin films using a polymeric swelling agent. J Phys Chem C 115:11925–11933. doi:10.1021/jp2021193

Xu H, Zhang L (2009) Controllable one-pot synthesis and enhanced photocatalytic activity of mixed-phase TiO$_2$ nanocrystals with tunable brookite/rutile ratios. J Phys Chem C 113:1785–1790. doi:10.1021/jp8089903

Zana R, Marques C, Johner A (2006) Dynamics of micelles of the triblock copolymers poly(ethylene oxide)–poly(propylene oxide)–poly(ethylene oxide) in aqueous solution. Adv Colloid Interface Sci 123–126:345–351. doi:10.1016/j.cis.2006.05.011